Gelatinous matrix, an original strategy to cope with oligotrophy in Nassellaria (Radiolaria)

Short title: Radiolaria gelatinous matrix evolution.

Natalia Llopis Monferrer[1,2,*], Sarah Romac[1], Manon Laget[3,4], Yasuhide Nakamura[5], Tristan Biard[4,#], Miguel M. Sandin[6,*,#]

[1]Sorbonne University, CNRS, UMR7144 Adaptation and Diversity in Marine Environment (AD2M) Laboratory, Ecology of Marine Plankton team, Station Biologique de Roscoff, Roscoff, France
[2]Monterey Bay Aquarium Research Institute, Moss Landing, CA, United States
[3] Oceanography Department, Dalhousie University, Halifax, NS, Canada
[4]LOG, Laboratoire d'Océanologie et de Géosciences, Université du Littoral Côte d'Opale, Université de Lille, CNRS, IRD, UMR8187, Wimereux, France
[5]Estuary Research Center, Shimane University, 1060, Nishikawatsu-cho, Matsue-city, Shimane-ken, 690-8504 Japan
[6]Institut de Biologia Evolutiva (CSIC-Universitat Pompeu Fabra), Passeig Marítim de la Barceloneta 37-49, 08003 Barcelona, Spain
[#]Senior authors
[*]Corresponding authors

Natalia Llopis Monferrer
MCSA Postdoctoral Fellow
Monterey Bay Aquarium Research Institute
7700 Sandholdt Road
Moss Landing, CA 95039
nllopis@mbari.org

Miguel M. Sandin
Beatriu de Pinos Postdoctoral Fellow
Institut de Biologia Evolutiva (CSIC-Universitat Pompeu Fabra),
Passeig Marítim de la Barceloneta 37-49
08003 Barcelona, Spain
miguelmendezsandin@gmail.com

Abstract

Radiolaria are heterotrophic protists abundant in the world's oceans playing important roles in biogeochemical cycles. Some species host photosynthetic algae also contributing to primary production. Such mixotrophic behaviour is believed to explain their ecological success in oligotrophic waters, notably Collodaria, exclusively mixotrophic radiolarians within a gelatinous matrix. Yet, our understanding of Radiolaria ecology is limited to direct observations, as they have so far withstood reproduction in culture and their genomes are unexplored. Sampling oligotrophic California Current communities revealed an abundant, rarely observed population of Nassellaria of the genus *Phlebarachnium*, characterized to live within a gelatinous matrix along with other Radiolaria. Phylogenetic reconstruction of the ribosomal DNA suggests that these distantly related lineages within Nassellaria independently developed the ability to produce a gelatinous matrix ~150 million years ago. By matching physical samples with their genetic signature, we identified these rarely observed organisms in global metabarcoding datasets, revealing strong biogeographic affinity to oligotrophic water masses. Global ocean co-occurrence networks showed that Radiolaria with a gelatinous matrix have a distinct biogeography compared to those without the matrix. Results suggest that the gelatinous matrix is an adaptation to oligotrophic waters, but further research is needed to evaluate similarities between the gelatinous matrices across different Radiolaria groups. This strategy could increase the effective volume to weight ratio favoring prey capture and create a favorable microenvironment for symbionts, enhancing ecological success in nutrient-depleted waters. This study advances our understanding of eukaryotic diversity evolution, emphasizing specific advantages of certain adaptations, specifically when evolution occurs independently across lineages.

Keywords: Radiolaria, gelatinous matrix, evolution, symbionts

Introduction

Among marine planktonic eukaryotic organisms, Radiolaria are diverse and highly abundant protists, widely distributed in the ocean, from tropical to polar waters [1]. These protists exhibit a great range of lifestyles (solitary and colonial), trophic diversity (heterotrophic or mixotrophic bearing photosynthetic symbionts) and tremendous morphological variability, spanning a wide range of sizes, from micrometers to several millimeters [2, 3]. Among the phylogenetic groups of Radiolaria, Acantharia [4] is the sole group of Radiolaria bearing a strontium sulfate skeleton, while the Polycystines group possesses opaline silica skeletons [5]. In the Polycystines group, Spumellaria [6] exhibits concentric and spherical shapes, while Nassellaria [7] showcases a diverse range of features. These include conical skeletons and a limited number of spicules, or even large colonies, akin to that found in the Collodaria group [8], or large individual skeletons as found in the Orodaria group [9]. This extensive diversity makes Radiolaria an ideal lineage for investigating adaptive evolution in protists.

Additionally, Radiolaria have successfully adapted to diverse ocean environments and are found at various depths, being important contributors to contemporary biogeochemical cycles. They can participate in the transformation of sinking particles and have been identified as a critical source of organic carbon [10, 11]. Global estimates indicate that Rhizaria, including Collodaria among other protists, may constitute up to 20% of the biomass of the euphotic layer (0-200m) [12]. They also play a substantial role in zooplankton abundance, contributing up to 33% [1]. In some areas, Radiolaria may dominate the eukaryotic community recovered from metabarcoding analyses of sediment traps based below the euphotic layer [13, 14]. They also have an essential role in the silicon cycle, as many representatives take up silicic acid from the seawater to form their skeleton [15] contributing approximately 20% to the biogenic silica production of the global ocean [16]. It is because of their intricate mineral skeleton made of opaline silica that Radiolaria have left behind

70 a continuous fossil record since the Cambrian, more than 500 million years ago (Mya) [17], and
71 have been instrumental for paleoenvironmental reconstructions [18, 19].

72 Due to the challenges of collecting these protists intact, the difficulty of maintaining them in culture,
73 and the lack of information about their genomes, most of our current understanding about their
74 ecology is derived from isolated and random observations in the field. Notably, various types of
75 trophic modes and feeding strategies have been observed in Radiolaria. Some feed upon sinking
76 particles while others are active predators or exhibit a combination of both behaviors. They use a
77 network of cytoplasmic extensions (i.e., pseudopods) to capture and entangle a wide range of
78 prey, from bacteria to multicellular heterotrophs like nauplii larvae [2, 20], even in oligotrophic
79 waters where prey abundance is scarce. Many are mixotrophs harboring photosynthetic algae
80 [21–23]. These symbionts can be found either directly inside the cell membrane as in Acantharia
81 [24], or scattered on a gelatinous organic matrix surrounding the skeleton as in Collodaria [25].
82 The presence of photosymbionts in these organisms contributes to primary production. In the
83 upper 20 m of the central North Pacific, Acantharia alone can contribute up to 4% of total primary
84 production and up to 20% of surface production [26, 27]. It has been suggested that such
85 symbiotic adaptations were triggered by long periods of accentuated oceanic oligotrophy in the
86 Jurassic (ca. 175-93 Mya; [4]).

87 In contemporary oceans, mixotrophy allows Radiolaria to thrive in various environments.
88 Collodaria are an important component of zooplankton biomass in the epipelagic and are most
89 abundant in tropical latitudes and nutrient-impoverished waters [28]. Conversely, other Radiolaria,
90 such as Acantharia or Spumellaria, are better adapted to meso- and eutrophic waters, richer in
91 nutrients. These differences in biogeographical patterns have been attributed to the coloniality of
92 Collodaria in which all individual cells share nutrients among the colony through the gelatinous
93 matrix [25].

The presence of the gelatinous envelope surrounding the cell [29] could be a crucial advantage in enabling them to survive and thrive abundantly in oligotrophic waters, where prey are scarce. The gelatinous matrix also provides a conducive environment for hosting symbionts while facilitating resource optimization and adaptation strategies that contribute to the survival and ecological success of the cell. Indeed, other marine organisms, such as *Phaeocystis* algae, can also form an extracellular matrix that can host bacteria [30, 31], providing a nutrient-rich and protective environment and allowing them to form blooms and dominate the planktonic community.

In an oligotrophic environment, we collected several Nassellaria specimens embedded in a gelatinous matrix. To our knowledge, only one other study has documented these specimens, originally described as *Sethoconus myxobrachia* [32], yet recently reassigned to the genus *Phlebarachnium* [33]. The study of these rare specimens offers a unique opportunity to investigate the presence of the gelatinous matrix, a trait that may be vital for adaptation to new environmental conditions, allowing us to formulate new hypotheses to better understand evolutionary processes in protists. We present here findings on the phylogenetic relationships and global biogeography of *Phlebarachnium*. Our approach involved sequencing rDNA genes, characterisation of the surrounding waters where these specimens were collected, and the analyses of metabarcoding datasets (Eubank; [34]). Here we hypothesize that the gelatinous matrix serves as an ecological adaptation to oligotrophy, as we observed it evolved independently in different groups of Nassellaria. This gelatinous matrix would increase cell volume, facilitating the capture and storage of scarce prey and nutrients. Additionally, it offers larger cellular space to host an increased number of symbionts providing an optimal environment for them, here identified within the genus *Scrippsiella*.

Material and Methods

Sample collection

Samples were collected during the P2107 California Current Ecosystem Long Term Ecological Research (CCE-LTER) cruise in the summer of 2021 aboard the R/V *Roger Revelle* (Fig. 1A). The sampling strategy was designed around 3 multi-day quasi-lagrangian cycles. Each cycle involved following the drift trajectories of experimental arrays, aiming to sample the same water mass. Individual casts of Conductivity, Temperature and Depth (CTD) were conducted at each station (~about 10 per cycle). Discrete bottle samples were collected at various depths from each station to measure nutrients (silicic acid ($Si(OH)_4$) and nitrate (NO_3^-)). Water column nutrient samples were measured following the standard operating procedures from the CCE-LTER. Briefly, macronutrient samples were collected and filtered through a 0.2-µm capsule filter before being frozen at -20°C for on-shore autoanalyzer analysis.

In this study, we present results from a subset of 4 stations of Cycle 3 (3-6 August), sampled in oligotrophic waters, where Nassellaria identified as *Phlebarachnium* sp. according to [32] were found (**Sup Fig. S1**). Plankton samples were collected using a ringnet (200-µm mesh size, mouth diameter: 1 m) towed vertically from 50 m to the surface, from 300 m to the surface and from vertically stratified sampling collected with a 1-m^2 opening, 202-µm mesh MOCNESS.

Immediately after collection, each net sample was observed using a stereomicroscope (Zeiss Stemi 508) and images of targeted organisms were captured using a Canon Eos 77D camera. Morphological measurements, including major and minor axes of individual cells, and their skeleton area, were obtained using ImageJ software [35, 36] to estimate the biovolume of the cells (Equations 1 and 2) (**Sup Table S1**). Each specimen was transferred into 1.5-ml Eppendorf tubes containing 50 µl of molecular grade absolute ethanol and stored at -20˚C until DNA extraction. Scanning electron microscopy images were captured using a S-3400N Hitachi

141 scanning electron microscope following the protocol in [37] for detailed examination of
142 morphology.

143 $$volume = \frac{4}{3} \cdot \pi \cdot \frac{major}{2} \cdot \frac{minor}{2} \cdot \frac{minor}{2} \quad \text{(Eq. 1)}$$
144

145 $$ESD = 2 \cdot \left(\frac{3}{4} \cdot \frac{volume}{\pi}\right)^{\frac{1}{3}} \quad \text{(Eq. 2)}$$

146 # DNA extraction and sequencing

147 DNA was extracted using the MasterPure Complete DNA and RNA Purification Kit (Epicentre)
148 following the manufacturer's instructions. Partial 28S rDNA (D1 and D2 regions) was amplified by
149 Polymerase Chain Reaction (PCR) using Radiolaria and Nassellaria specific primers (28S-Nas-
150 F: 5' - AGT AAC GGC GAG TGA AGC - 3' and 28S-Nas-R: 5' - CCA ACA TAC DTG CTC TTG T
151 - 3'). For further details about rDNA amplification see {Citation}. PCR amplicons were visualized
152 on 1% agarose gel stained with ethidium bromide. Positive reactions were purified using the
153 Nucleospin Gel and PCR Clean up kit (Macherey Nagel), following manufacturer's instructions
154 and sent to Macrogen Europe for sequencing. After sequencing, forward and reverse sequences
155 were checked and assembled using ChromasPro software version 2.1.4 (2017). Sequences were
156 compared to the GenBank reference database using the BLAST search tool integrated in
157 ChromasPro to discriminate radiolarian sequences from possible contamination. The presence of
158 chimeras was checked by mothur v1.39.3 [38] against the PR2 database v5.0. [39]. No chimeras
159 were found, and therefore sequences were kept for further analyses. Final sequences were
160 deposited in NCBI under the accession numbers OR978667-OR978672. Single-cell amplification
161 and sequencing of the 18S rDNA was also attempted following [7], yet after checking correct *in*
162 *silico* specificity of the primers, no successful reactions yielded 18S sequences of the Nassellaria
163 host and DNA template was spent before achieving successful amplification.

164 # Phylogenetic analysis

165 Our partial 28S rDNA sequences were compared against an environmental dataset [40]
166 containing near full-length sequences of the rDNA (from doi: 10.6084/m9.figshare.15164772.v3)
167 using the '--usearch_global' option from vsearch v2.21.1 [41]. In total 2 sequences of the near
168 full-length rDNA were identified with a similarity identity of 99.8%, with the third best identity score
169 at 89.1%. Additionally, 135 Nassellaria sequences were extracted from [42], with 24 Spumellaria
170 sequences as the outgroup (**Sup Table S2**). Datasets of the 18S and 28S rDNA were
171 independently aligned with mafft [43] using the L-INS-i algorithm ('—localpair') and 1000 iterative
172 refinement cycles. The alignment was visualized in AliView v1.28 [44] to check for possible
173 artifacts and trimmed with a 5% gap threshold using trimAl [45]. Final alignments contained 151
174 sequences with 1849 aligned positions for the 18S rDNA and 93 sequences with 800 positions
175 for the partial 28S rDNA. Final datasets of the 18S and the partial 28S rDNA were concatenated
176 with an in-house script freely available on GitHub (MiguelMSandin/random/fasta/fastaConcat.py),
177 resulting in 165 sequences, 2647 aligned positions. Phylogenetic analyses were performed using
178 Maximum Likelihood (ML) implemented in RAxML-ng [46] and IQ-Tree [47] and a Bayesian
179 Inference (BI) implemented in MrBayes [48]. RAxML-ng was run under a GTR + Gamma model
180 of evolution over 100 parsimonious starting trees and 1000 Felsenstein bootstraps. Prior to
181 phylogenetic inference with IQ-Tree, ModelFinder identified GTR + F + R4 as the best fitting model
182 of evolution and it was therefore used over 1000 bootstraps and 10 independent runs. Lastly,
183 MrBayes was run under a GTR + Gamma model of evolution over 10 million generations and 4
184 independent runs. After checking for convergence of the bayesian MCMC chain in tracer v1.7.2
185 a 25% burnin was applied and a strict consensus tree was built.

186 While attempting 18S rDNA amplification, up to 6 different and high-quality sequences
187 taxonomically assigned to dinoflagellates were sequenced from 6 independent hosts (deposited

188 in NCBI under the accession numbers OR961112-OR961117). These sequences were combined
189 with those used in [21] in order to study the phylogenetic relationships of the potential symbionts.
190 In total 71 sequences of the 18S rDNA were aligned and trimmed (following methods stated
191 above) resulting in 1803 positions. Phylogenetic analyses were inferred in RAxML-ng and IQ-
192 Tree as mentioned above.

193 Calibration of the molecular clock

194 Divergence times among sequences were estimated in BEAST v2.7.3 [49] under the Optimized
195 Relaxed Clock [50] model to avoid assumption of substitution rates correlation between sister
196 clades, a GTR+Gamma (4 categories) model of nucleotide substitution and a Birth-Death model
197 of speciation [51]. Fossil calibrations were taken from [42], including a maximum root age of 1200
198 Mya and minimum of 500 Mya under a uniform distribution. The Bayesian MCMC chain was run
199 over 10 million generations sampled every 1000 states on 3 independent runs (remaining
200 operators were left as default). After completion, effective sampling size was checked to be equal
201 or higher than 200 and the 3 independent runs were combined in LogCombiner v2.7.4 with a 25%
202 burnin. The final tree was summarized in TreeAnnotator v2.7.3.

203 Ancestral state reconstruction

204 We reconstructed ancestral states for the Nassellaria clade to infer whether the gelatinous matrix
205 is an acquired trait or instead an ancestral trait. To do so, two complementary approaches were
206 carried out over the resulting time calibrated tree. The first approach was performed under a
207 Maximum Likelihood (ML) Binary State Speciation and Extinction model (BiSSE) implemented in
208 the R package ‘diversitree’ v0.10 [52], with the functions ‘make.bisse’ and ‘find.mle’. Phylogenetic
209 tips known for the presence or absence of gelatinous matrix [33] received a ‘1’ or a ‘0’,
210 respectively, while environmental sequences with unknown morphology were assigned an empty

211 value (i.e., 'Not Available': 'NA'). All families described with the presence of a gelatinous matrix in
212 [33] were represented in our dataset. The second approach followed a Bayesian Inference (BI)
213 implemented in BEAST2 performed under a birth death model with 10 million generations
214 sampled every 1000 steps and a 25% burnin. As for the ML approach, phylogenetic tips whose
215 presence or absence of gelatinous matrix are known were given their respective categorical
216 values. However, this approach does not allow the absence of character traits and thus those
217 phylogenetic tips whose morphology is unknown were given a third categorical value. After such
218 a limitation, the ML approach was chosen as principal analyses and the BI approach was used
219 for assessing consistency of results and our dataset.

220 Global biogeographic analyses

221 Global biogeographic patterns of *Phlebarachnium* were examined in the EukBank metabarcoding
222 dataset of the V4 hypervariable region of the 18S rDNA [34] accessed at doi:
223 10.5281/zenodo.7804946. *Phlebarachnium* metabarcodes were extracted from the near-full
224 length rDNA sequences mentioned above with the '--usearch_global' option from vsearch v2.21.1
225 [41] and default parameters. In total, 2 metabarcodes from the V4 rDNA were selected and
226 extracted from the EukBank dataset with a similarity identity of 99.5% and 96.9% (the third closest
227 metabarcode hit to our *Phlebarachnium* sequences had an identity of 89.4%). Given that the
228 abundance of the second metabarcode was significantly lower than that of the first metabarcode
229 (14 total reads compared to 306522), read abundances of both metabarcodes were clustered
230 together for biogeographic patterns exploration. Only samples with a marine identifier under
231 'biome' were considered in this study.

232 Co-occurrence networks

233 To understand whether the presence of the gelatinous matrix has ecological implications or not,
234 we reconstructed co-occurrence networks for all Radiolaria amplicons worldwide from the
235 previously described dataset (EukBank). Network inference was performed using FlashWeave
236 v0.19 [53], a recently developed tool to accommodate data compositionality and infer statistical
237 co-occurrence or co-abundance interactions. All Radiolaria amplicons with known presence or
238 absence of a gelatinous matrix were extracted from the OTU table, and samples with no
239 Radiolaria reads were discarded. To avoid potential over-clusterization of intragenomic variability,
240 PCR/sequencing errors and other artifacts [54], we only considered amplicons with a maximum
241 relative abundance in any given sample of at least 1%. FlashWeave applies a centered log-ratio
242 (CLR) transformation prior to inferring local-to-global learning framework, and thus no additional
243 transformations were used. Given the relatively large proportion of amplicons assigned to
244 undescribed groups of Radiolaria (such as RAD-A, RAD-B, RAD-C or environmental clades within
245 e.g., Collodaria), analyses were then replicated also considering amplicons whose gelatinous
246 state is unknown. In addition, given the large size ranges of gelatinous Radiolaria (from few µm
247 to several cm), supplementary analyses were run on specific size fractions in order to account for
248 possible sampling biases. In total, 945 Radiolaria amplicons were considered of which 244 were
249 assigned to Radiolaria with a gelatinous matrix, 319 to Radiolaria without a gelatinous matrix and
250 382 had an unknown attribute. From the 563 amplicons with known attributes, 547 were found
251 only in the small size fraction (0.22-20 µm), 501 in the medium size fraction (3-200 µm), and 495
252 in the large size fraction (80-2000 µm or bigger). Such overlap between different size-fractions
253 groups was a result of the large variability of sampling approaches covered across the EukBank
254 dataset.
255 Two additional analyses were applied over the resulting networks to better understand community
256 structure and co-occurrence: The assortativity of the gelatinous attribute and Louvain clusters.
257 The assortativity coefficient measures the preference of nodes with a given attribute to be
258 connected to other nodes with the same attribute, and it was calculated using the function

259 ‘attribute_assortativity_coefficient’ from the Python package ‘networkx’ v2.2 [55] implemented in
260 the custom script netAssortativity.py (publicly accessible at
261 github.com/MiguelMSandin/random/networks/). To test the significance of the assortativity values
262 and the probabilities of deviating from random assortativities, we randomize the gelatinous
263 attributes 100 times over the exact same network and compare the original assortativity value
264 with those obtained from randomization with a one-sample T-test. The second analysis, the
265 Louvain method, implements the multi-level modularity optimization algorithm for finding
266 community structure in a hierarchical approach to extract non-overlapping communities or
267 clusters. Louvain clusters were estimated with the ‘cluster_louvain’ function from the R package
268 ‘igraph’ v2.0.3 [56] and a 0.5 resolution parameter since it was the value that best explained
269 community structure by keeping small clusters yet sufficiently large to be meaningful regarding
270 our initial question. All networks were visualized in Cytoscape v3.10.2 [57] after applying an
271 organic layout.

272 Results

273 Environmental context

274 Specimens of *Phlebarachnium* were found in highly oligotrophic waters, where Chlorophyll *a*
275 concentration was low (ranging from 0 to 9 mg m^{-3}) (Fig. 1A). At Cycle 3, fluorescence values
276 were almost negligible, except for a peak detected at around 100 m (Fig. 1B). In Cycles 1 and 2,
277 near the coast, fluorescence and Chlorophyll *a* values were much higher in the upper 100 m of
278 the water column than in Cycle 3. Nutrient concentrations (silicic acid and nitrate) in Cycles 1 and
279 2 showed an upward trend with depth from the surface waters. During Cycle 3, nutrients depletion
280 was observed in the upper 150 m of the water column. Beyond this depth, values reached 30 and
281 25 μM for silicic acid and nitrate, respectively.

Morphological assessment

Based on live observations and light microscope images, two populations of *Phlebarachnium* cells were defined showing differences in average size, color and depth distribution, which we refer to as the yellow and orange populations (Fig. 2A and B, respectively). Both populations were surrounded by a gelatinous matrix. Morphometric assessments of matrix and skeleton, including major and minor axes measurements, volume and estimated spherical diameter (ESD) calculations, were conducted on 25 individuals from each population (**Sup Table S1**). The ESD of the gelatinous matrix was 845 (± 73) µm and 1383 (± 129) µm, and the skeleton ESD was 332 (± 35) µm and 563 (± 49) µm for the yellow and orange populations, respectively. A Wilcoxon test indicated that both matrix and skeleton in orange specimens were significantly larger than yellow specimens ($Z=-4.37$, pvalue<0.001; $Z=-4.37$, pvalue<0.001). The skeleton volume/matrix ratio volume varied from 3 to 12%, with no significant differences among populations ($Z=-1.70$, pvalue=0.09).

In approximately 15% of the specimens from the yellow population collected, we observed the presence of enclosed prey within the gelatinous matrix. These include mainly harpacticoid copepods and nauplius larvae. All copepods were consistently placed near the aperture (Fig. 2C, dashed white arrow), and on many occasions we observed a clear opening within the gelatinous matrix (Fig. 2C, solid white arrow). Although we cannot conclude on the vertical distribution of these organisms due to sampling limitations, we observed some distribution patterns in depth. While host specimens of the yellow population were found in all the nets tows, from 0-50 m, from 75-150 m and 0-300 m, specimens of the orange population were only found in the deeper net tows, below 75 m.

Both populations show numerous golden-yellow bodies distributed across the gelatinous matrix, with a lower concentration in the deeper-dwelling orange population. Both populations show

306 different distributions of these golden yellow bodies. In the yellow population, they appear
307 arranged in clusters within specific and recurring regions of the matrix, which may show rounded
308 inflations. We noted the presence of 3 to 4 clusters of symbionts, with one positioned toward the
309 apical horn and 2 to 3 arranged toward the bottom of the gelatinous matrix (**Fig. 2A**). In contrast,
310 in the orange population, symbionts are evenly distributed throughout the matrix (**Fig. 2B**).
311 Despite differences in skeleton size and symbionts distribution, both populations shared common
312 features in their skeletal morphology. Each representative exhibited a reticulate shell,
313 characterized by a spherical cephalic region and a larger bell-shaped thorax (**Fig. 2D-G**).

314

315 Molecular and phylogenetic analyses

316 Phylogenetic analyses revealed that *Phlebarachnium* constitute a highly supported novel clade
317 (Bootstrap Support, BS≥94; Posterior Probability, PP≥0.91) within Nassellaria and confidently
318 supported (BS=72 and 78, PP=0.98) as sister to Lithochytridoidea, Pterocorythoidea and an
319 environmental clade (a clade with no morphologically described sequences) named as Nass-4
320 (**Fig. 3**).
321 This distinct *Phlebarachnium* clade shows a distant phylogenetic relatedness to Orodaria,
322 Collodaria and the other family within Acanthodesmioidea that also develops a gelatinous matrix
323 around the cells. Molecular dating estimates the last common ancestor between *Phlebarachnium*
324 and Collodaria in 337 Mya (with a Highest Posterior Density -HPD- between 415 and 270 Mya;
325 **Fig. 4**). Orodaria and Collodaria diversified 166 Mya (HPD: 223-115). While Collodaria has been
326 dated to first diversified at 134 Mya (HPD: 185-92), *Phlebarachnium* clade first diversified 5.4 Mya
327 (HPD: 13.8-1.1), yet separated from its sister clades much earlier at 127 Mya (HPD: 187-84), and
328 Orodaria only diversified 1.3 Mya (HPD: 6.4-0.01).
329 Ancestral state reconstruction analyses confidently support an independent development of the
330 gelatinous matrix in *Phlebarachnium*, the group of Collodaria and Orodaria, and the family

Cephalospyrididae within Acanthodesmioidea (**Fig. 4**). The reconstructed last common ancestor between all gelatinous groups had no gelatinous matrix and such state was fully supported in both maximum likelihood and Bayesian inference. However, given the amount of undescribed diversity (especially within Collodaria), Bayesian inference failed to reconstruct a state for the last common ancestor between Orodaria and Collodaria (**Sup Fig. S2**) with 0.48 Posterior Probabilities (PP) of an unknown state over 0.47 PP for a gelatinous state and 0.05 PP for a non-gelatinous state. The gelatinous matrix could have evolved independently in Collodaria and Orodaria, and thus the first appearance of the gelatinous matrix could have either be with the diversification of Orodaria and Collodaria (at ~166 Mya; or earlier) or with that of Collodaria (at ~134 Mya), nearly matching the divergence of *Phlebarachnium* with their sister groups (at ~127 Mya).

While morphological observations identified two distinct populations, molecular analyses showed no clear differentiation as all sequences obtained in our study were identical. Environmental molecular diversity from the different datasets studied herein also showed limited diversity, agreeing on a unique molecular marker of *Phlebarachnium*, despite the different lengths (near full-length rDNA) and sequencing depth (accounting for intragenomic variability) considered in the respective environmental datasets. In addition, both populations show similar golden yellow bodies phylogenetically assigned to *Scrippsiella* (**Sup Fig. S3**), a dinoflagellate frequently found in symbioses with other organisms, yet independent of Polycystines's common symbiont, *Brandtodinium*.

Biogeographic analyses

Overall, the collection and identification of this enigmatic Radiolaria in the California Current allowed for the identification of a previously unassigned sequence in a global metabarcoding dataset. Here, we have used different sequences coming from various sources to explore global biogeographic patterns of *Phlebarachnium*, and due to their high degree of similarity (>96.9%) and the pairwise distance dissimilarity to other non-*Phlebarachnium* sequences (<89.4) we were

356 confidentially able to taxonomically assign these reads to *Phlebarachnium* (**Fig. 5D**). Global
357 metabarcoding analysis of the V4 hypervariable region of the rDNA shows that *Phlebarachnium*
358 contributed on average 0.45 (±1.4) % to the total eukaryotic community across the EukBank
359 dataset (with a median contribution of 0.02%). Yet in some samples of the Pacific Ocean,
360 *Phlebarachnium* contributes to up to 13.41% of the total eukaryotic reads (**Fig. 5A**). The Pacific
361 Ocean accounted for the majority of *Phlebarachnium reads*, gathering more than 96% of the total
362 *Phlebarachnium* relative reads and nearly half of the samples where *Phlebarachnium* was present
363 (75 of 162 global samples of which in 58 showed a relative abundance of at least 2% to the total
364 eukaryotic reads). The highest relative abundance of *Phlebarachnium* coincided with the
365 oligotrophic gyres of the Pacific Ocean at ~30° of latitude (**Fig. 5B**) and in between -80° and -
366 180° of longitude of the upper mesopelagic water mass (200-1000 m; **Fig. 5C**).

367 Co-occurrence network analyses showed a strong correlation in the biogeography of gelatinous
368 Radiolaria with other gelatinous Radiolaria and similarly for non-gelatinous Radiolaria co-
369 occurring with non-gelatinous Radiolaria (**Fig. 6**). Such a pattern received an assortativity
370 coefficient of 0.79, with a p-value of 0 (**Fig. 6A**). Louvain clusters identified three communities, of
371 which two tended to contain amplicons that show a higher abundance towards the surface
372 whereas the third community showed amplicons co-occurring at deep samples (**Fig. 6B**). Among
373 the two shallow water communities one of them was constituted of primarily gelatinous Radiolaria
374 and was correlated with no environmental parameter. The second shallow community contained
375 primarily non-gelatinous Radiolaria and was positively correlated with nearly all environmental
376 parameters, especially with total eukaryotic ASV richness, meaning that these amplicons tend to
377 co-occur when samples are taxonomically diverse. The family Cephalospyrididae
378 (Acanthodesmioidea) are the only amplicons associated with a gelatinous matrix that appeared
379 in this cluster, and their maximum relative abundance is lower (with maximum relative
380 abundances of 9.1, 4.4, 2.1, 1.6 and 1.2%) compared to other amplicons with a gelatinous matrix

381 (e.g., *Phlebarachnium*: 13.41%). *Phlebarachnium* was in the third Louvain cluster and was
382 correlated with depth. Despite that only 18 amplicons correspond to gelatinous Radiolaria (from
383 142 amplicons) in the third cluster, this attribute still showed a significant assortativity coefficient
384 (0.27).

385 When breaking down co-occurrence patterns into different size fractions to account for possible
386 sampling biases, similar assortativity coefficients were found with 0.749, 0.646 and 0.734
387 coefficients for the small, medium and big size fractions respectively (**Sup Fig. S4**). In all different
388 size fractions, Louvain clusters that contained *Phlebarachnium* were never found to be correlated
389 with total ASV richness, and neither were other clusters containing primarily gelatinous amplicons.
390 Besides, *Phlebarachnium* showed correlations with deep samples only in the small size fractions,
391 while in the medium and big size fractions there is no such correlation. The inclusion of amplicons
392 with an unknown trait also confirmed the trend of gelatinous amplicons co-occurring with
393 gelatinous amplicons and non-gelatinous with non-gelatinous (**Sup Fig. S5**). Since an unknown
394 attribute cannot be given, it represents a third attribute and yet a significant artificial assortativity
395 coefficient of 0.298 (or 0.796 after removing the unknown trait) and three independent Louvain
396 clusters were also identified as in **Fig. 6**.

397 Given the strong statistical support for the contrasting co-occurrence of amplicons with a
398 gelatinous matrix and amplicons without a gelatinous matrix, we repeated these co-occurrence
399 networks analyses including only samples from the *Tara* Oceans expedition and similar patterns
400 were found (data not shown).

401 Discussion

402 Here, we identified the genus *Phlebarachnium*, a distinct Nassellaria clade showing a
403 characteristic gelatinous matrix surrounding the cells and highly abundant in oligotrophic waters.

404 *Phlebarachnium* is, to our knowledge, the only solitary lineage of Radiolaria with a gelatinous
405 matrix that has been reported to exhibit bloom-like growth in oligotrophic waters. Despite their
406 distant relationship within the Nassellaria group, *Phlebarachnium*, Orodaria and Collodaria share
407 the adaptation of producing a gelatinous matrix and affinity towards oligotrophic zones. Orodaria
408 is restricted to oligotrophic deep waters, predominantly found in the Pacific Ocean, and lacks
409 symbiotic algae within its gelatinous matrix [9]. Collodaria exhibits high abundance and diversity
410 in shallow, oligotrophic waters [58], a trait attributed to the presence of numerous symbionts
411 scattered in the gelatinous matrix of the colonies [28]. Other Radiolaria groups, such as
412 Acantharia, do not possess a gelatinous matrix but still host numerous photosymbionts [24]. Since
413 Acantharia are rarely found in oligotrophic waters, here we argue that the gelatinous matrix could
414 be a specific innovation to cope with nutrient-poor systems. The gelatinous matrix would increase
415 the volume-to-body weight ratio, facilitating the hosting of a larger number of symbionts and
416 establishing a particular microenvironment that favours the viability of these organisms under
417 conditions of nutrient depletion. Additionally, the increased volume-to-body weight ratio would
418 improve the chances of prey encountering and/or scavenging nutrients for mineralization of the
419 skeleton and/or symbiont nourishment. For non-photosymbiotic Orodaria, mostly found in the
420 mesopelagic, the gelatinous matrix may play an important role for buoyancy. Altogether, the
421 gelatinous matrix seems to be a convergent adaptation to oligotrophic waters, where other
422 Radiolaria relatives are rare.

423 Other protists have also developed sophisticated behaviors to enhance encounter rates. Some
424 dinoflagellates can build a mucosphere with the capacity to attract and immobilize diverse
425 microbes, facilitating subsequent prey selection [59]. In other Radiolaria groups, comparable
426 independent innovations in life mode and morphology have already been hypothesized and
427 documented. Nassellaria's closest relative, Spumellaria, experienced a substantial increase in
428 planar forms during the second half of the Mesozoic, (ca. 145 Mya), which is thought to have

429 resulted from low nutrient availability favoring an increase in the surface/volume ratio [8]. Here we
430 have shown that the development of the gelatinous matrix happened at nearly the same
431 geological time and we have attributed similar oligotrophic reasons. During the same geological
432 epoch, Acantharia, established a photosymbiotic relationship with the haptophyte *Phaeocystis*
433 also linked to extended periods of oligotrophy [4]. In such a relationship, photosymbionts of
434 Acantharia exhibit plastidal volumes 38-fold larger than those of free-living *Phaeocystis* [24].

435 In the case of Acantharia, their photosymbionts are located inside the cytoplasm [24], whereas
436 Collodaria harbors their photosymbionts scattered in the gelatinous matrix or located on the
437 capsules. To our knowledge, Collodaria has not been documented without symbionts [58].
438 Moreover, some Collodaria have been shown to control the physiology and perhaps the life cycle
439 of their photosymbionts to an extent [25]. In the yellow population of *Phlebarachnium* studied
440 here, the symbionts were arranged forming discrete clusters within the host's gelatinous matrix,
441 suggesting an active host-mediated placement. In contrast, in the orange population found living
442 at deeper water masses, the symbionts were evenly distributed throughout the matrix. Despite
443 morphological variations among *Phlebarachnium* specimens, DNA barcoding and environmental
444 molecular diversity showed almost identical sequences in all specimens studied here, with
445 differences across the rDNA significantly smaller than those found at the intragenomic level [54].
446 This could also suggest that there exist various morphotypes in the same species. The co-
447 occurrence network analyses showed a depth profile of *Phlebarachnium* where the smallest size-
448 fractions correlate with deep samples, and larger size fractions tend to co-occur at the surface. It
449 is believed that small bi-flagellated cells (called swarmers), released by mature cells, play a role
450 in the reproductive cycle of Radiolaria [60, 61], and therefore such morphological plasticity and
451 symbiont relocation might represent different life-stages. Regardless of morphological
452 differences, all specimens of *Phlebarachnium* hosted round, golden-yellow bodies scattered in
453 the gelatinous matrix. Molecular analyses identified such bodies as *Scrippsiella* (Peridiniales,

454 Dinophycea), a common planktonic symbiont of the jellyfish *Velella velella* [62] and also seen in
455 symbiosis with Acantharia [4], but never before reported in Polcystines Radiolaria [21, 22].
456 However, given the broad symbiotic interactions among the Dinophycea group and the long
457 divergence time of *Phlebarachnium* (~127 Mya to the last common ancestor of the closest
458 relative), it is plausible that they developed a symbiotic relationship with a different group.

459 In addition to playing a central role in resource acquisition and harbouring symbionts, the matrix
460 also could be important for prey capture. Nassellaria are known to have cytoplasmic extensions
461 (pseudopods) that emerge from the conical cephalis, forming a web of cytoplasmic filaments
462 where prey are captured [63]. The presence of the extracellular matrix likely provides the cell with
463 greater motility and flexibility compared to cells lacking this matrix, facilitating predation on other
464 cells. In many of the collected specimens, we observed the formation of a hole in the matrix,
465 containing enclosed prey, predominantly copepods of the order Harpacticoida and nauplius
466 larvae. Pelagic harpacticoids, such as *Microsetella* sp., are often associated with marine snow
467 and aggregates in offshore areas where suspended food is scarce, similar to the waters where
468 the *Phlebarachnium* specimens of this study were collected. The consistent occurrence of prey in
469 the gelatinous matrix beneath the cephalis suggests that *Phlebarachnium* may play a relevant
470 role in pelagic food webs by preying on metazoan taxa. This is particularly notable in oligotrophic
471 waters, where *Phlebarachnium* seems to be endemic and prey are scarce.

472 In our study we found *Phlebarachnium* in high relative abundances in oligotrophic waters, even
473 in specimens collected at deeper depths (0-300 m). Metabarcoding analyses show that
474 *Phlebarachnium* reaches high relative abundances in the mesopelagic zone (200-1000 m), where
475 light penetration is limited and possibly insufficient for the functionality of the symbionts'
476 photosynthesis. Taking into account the significant high relative abundance below 500 m around
477 -160° longitude, this implies that these organisms may be versatile, thriving solely through
478 heterotrophy without relying on photosynthesis. However, oligotrophic clear waters display

479 relatively deep chlorophyll maxima (Fig. 1B) and thus photosynthesis is found at deeper
480 environments regarding nutrient enriched waters. Collodaria has already been shown to inhabit
481 ocean areas where other Radiolaria relatives are rare [42]. In tropical and subtropical nutrient-
482 depleted surface waters, Collodaria can reach up to 1.6×10^4 - 2.0×10^4 colonies per m^3 [64, 65].
483 In our study, *Phlebarachnium* sequences reached maximum abundances of 13.4% relative to the
484 total eukaryotic community reads, especially towards the upper mesopelagic. In this context,
485 *Phlebarachnium* likely thrives in deeper water layers than Collodaria, establishing a distinct
486 ecological niche. The access to this environment allowed them to become important contributors
487 to the planktonic food web of an ecosystem with potentially low predators. However, caution is
488 required when interpreting metabarcoding data [66, 67]. Life cycle of Radiolaria remains poorly
489 understood, and the same metabarcoding reads might reflect different life-stages (as previously
490 discussed) or it might happen that dead cells are incorporated into sinking particles [68].

491 The high abundance and local endemism of *Phlebarachnium* to oligotrophic waters makes them
492 useful candidates for paleoenvironmental reconstruction studies. Their bloom-like presence might
493 reflect an important role in biogeochemical cycles. Considering climate change and expansion of
494 oligotrophic waters in certain oceanic regions [69], the gelatinous matrix could be an enormous
495 advantage for these organisms. Specializing in resource-poor waters could allow *Phlebarachnium*
496 to expand into novel ecological niches, such as different habitats or trophic modes and adapt to
497 novel environmental conditions. It has already been observed that ocean warming can trigger
498 major shifts in the geographic distribution due to the combined effects of warming, stratification,
499 light, nutrients and predation, in a wide range of organisms, from phytoplankton to mammals [70,
500 71]. In fact, the extensive fossil record of Radiolaria has already shown that rapid climate changes
501 can lead to extinction of specific groups [72]. It is therefore critical to understand whether
502 adaptations, such as the development of a gelatinous matrix, can help certain organisms cope

503 with the rapid changes in ocean chemistry and temperature expected due to anthropogenic
504 activity.

505 Our study highlights that the presence of a gelatinous matrix in *Phlebarachnium* could be an
506 original strategy to cope with oligotrophy in the oceans. Studying the exact role of the matrix in
507 these organisms is of particular importance to better understand biodiversity and adaptation of
508 Radiolaria. In particular, investigating the genes responsible for its formation and its chemical
509 composition (i.e., the amount of lipids and carbohydrates) may help to further understand its
510 relationship with symbionts, prey and the host cell. However, both the genomes of Radiolaria and
511 their reproduction in culture have so far withstood our efforts, which complicates further
512 investigations with traditional or conventional techniques. That is why these observations, despite
513 being random, are crucial, allowing us to hypothesize that the gelatinous matrix might be an
514 advantageous trait to adapt to oligotrophic conditions by increasing the effective body size and
515 creating an advantageous microenvironment for symbionts. Such increase in size might thus
516 allow them to host more photo-symbionts than their relatives without a gelatinous matrix and
517 similar body weight and further digest prey. This study not only advances our understanding in
518 the ecological strategies of Radiolaria but also offers insights into the broader dynamics of
519 organisms flourishing in nutrient-limited ecosystems.

520

Author contributions

NLM and ML collected the samples. NLM and MMS conceived the presented idea, participated in the conceptualization, planned and performed the analyses, prepared the figures and wrote the manuscript. SR carried out the DNA extraction, amplification and purification. NLL, ML, SR, YN, TB and MMS commented and revised the manuscript.

Acknowledgments

The authors would like to thank the captain and crew of the R/V *Roger Revelle* of the Scripps Institution of Oceanography for their expertise and support. We also thank colleagues within the CCE-LTER program (National Science Foundation grants OCE-1637632 and OCE-1614359) who contributed to sample collection and its lead PIs Katherine Barbeau and Mark Ohman. This work was supported by the “Agence Nationale de la Recherche” project RhiCycle (ANR-19-CE01-0006) granted to TB and the ISblue project RHICE (ANR-17-EURE-0015). NLL received funding from the European Union’s Horizon Europe research and innovation programme under grant agreement No 101064167 (MSCA postdoctoral fellowship Si-ORHIGENS). MMS was supported by a postdoctoral fellowship from the Beatriu de Pinós programme of the Government of Catalonia's Secretariat for Universities and Research of the Generalitat de Catalunya Economy and Knowledge (grant number: 2021BP00068). We would like to express our gratitude to Aude Leynaert for support, Fabrice Not for providing lab space and resources, ABiMs for computational resources, Johan Renaudie for the taxonomic contribution, Nicolas Henry for advising us on biogeographic analyses, Ian Probert for discussions on the nature of the symbionts and Steve Cunningham for SEM support. We are also very grateful to Colleen Durkin and Daniel Richter for their valuable input and advice on earlier versions of this manuscript. We thank two anonymous reviewers for their valuable contributions to improving the manuscript.

544 **Conflict of Interest Statement:** We have no conflicts of interest to disclose.

545 **Data availability:** The datasets generated during and/or analysed during the current study were
546 deposited in NCBI and are available under the accession numbers OR978667-OR978672 and
547 OR961112-OR961117. The environmental datasets used were accessed from doi:
548 10.6084/m9.figshare.15164772.v3 and 10.5281/zenodo.7804946.

References

1. Biard T, Stemmann L, Picheral M, Mayot N, Vandromme P, Hauss H, et al. In situ imaging reveals the biomass of giant protists in the global ocean. *Nature* 2016; **532**: 504–507.
2. Suzuki N, Not F. Biology and Ecology of Radiolaria. *Marine protists: diversity and dynamics*. 2015. Springer, Tokyo; New York, pp 179–222.
3. Biard T. Rhizaria. *eLs* 2022.
4. Decelle J, Suzuki N, Mahé F, De Vargas C, Not F. Molecular Phylogeny and Morphological Evolution of the Acantharia (Radiolaria). *Protist* 2012; **163**: 435–450.
5. Takahashi K. Radiolaria: sinking population, standing stock, and production rate. *Marine Micropaleontology* 1983; **8**: 171–181.
6. Sandin MM, Biard T, Romac S, O'Dogherty L, Suzuki N, Not F. A Morpho-molecular Perspective on the Diversity and Evolution of Spumellaria (Radiolaria). *Protist* 2021; **172**: 125806.
7. Sandin MM, Pillet L, Biard T, Poirier C, Bigeard E, Romac S, et al. Time Calibrated Morpho-molecular Classification of Nassellaria (Radiolaria). *Protist* 2019; **170**: 187–208.
8. Biard T, Pillet L, Decelle J, Poirier C, Suzuki N, Not F. Towards an Integrative Morpho-molecular Classification of the Collodaria (Polycystinea, Radiolaria). *Protist* 2015; **166**: 374–388.
9. Nakamura Y, Tuji A, Kimoto K, Yamaguchi A, Hori RS, Suzuki N. Ecology, Morphology, Phylogeny and Taxonomic Revision of Giant Radiolarians, Orodaria ord. nov. (Radiolaria; Rhizaria; SAR). *Protist* 2021.
10. Lampitt RS, Briggs N, Cael BB, Espinola B, Hélaouët P, Henson SA, et al. Deep ocean particle flux in the Northeast Atlantic over the past 30 years: carbon sequestration is controlled by ecosystem structure in the upper ocean. *Front Earth Sci* 2023; **11**: 1176196.
11. Laget M, Drago L, Panaïotis T, Kiko R, Stemmann L, Rogge A, et al. Global census of the significance of giant mesopelagic protists to the marine carbon and silicon cycles. *Nat Commun* 2024; **15**: 3341.
12. Drago L, Panaïotis T, Irisson J-O, Babin M, Biard T, Carlotti F, et al. Global Distribution of Zooplankton Biomass Estimated by In Situ Imaging and Machine Learning. *Front Mar Sci* 2022; **9**: 894372.
13. Gutierrez-Rodriguez A, Stukel MR, Lopes dos Santos A, Biard T, Scharek R, Vaulot D, et al. High contribution of Rhizaria (Radiolaria) to vertical export in the California Current Ecosystem revealed by DNA metabarcoding. *ISME J* 2018; **13**: 964–976.
14. Preston CM, Durkin CA, Yamahara KM. DNA metabarcoding reveals organisms contributing to particulate matter flux to abyssal depths in the North East Pacific ocean. *Deep Sea Research Part II: Topical Studies in Oceanography* 2020; **173**: 104708.
15. Llopis Monferrer N, Boltovskoy D, Tréguer P, Sandin MM, Not F, Leynaert A. Estimating Biogenic Silica Production of Rhizaria in the Global Ocean. *Global Biogeochem Cycles* 2020; **34**.
16. Tréguer PJ, Sutton JN, Brzezinski MA, Charette MA, Devries T, Dutkiewicz S, et al. Reviews and syntheses: The biogeochemical cycle of silicon in the modern ocean. *Biogeosciences* 2021.

17. De Wever P, Dumitrica P, Caulet JP, Nigrini C, Caridroit M. Radiolarians in the Sedimentary Record. 2001. CRC Press, London.
18. Lazarus D, Suzuki N, Ishitani Y, Takahashi K. Paleobiology of the Polycystine Radiolaria, 1st ed: Hoboken. 2021. NJ: Wiley-Blackwell.
19. Civel-Mazens M, Crosta X, Cortese G, Michel E, Mazaud A, Ther O, et al. Antarctic Polar Front migrations in the Kerguelen Plateau region, Southern Ocean, over the past 360 kyrs. *Global and Planetary Change* 2021; **202**: 103526.
20. Nakamura Y, Itagaki H, Tuji A, Shimode S, Yamaguchi A, Hidaka K, et al. DNA metabarcoding focused on difficult-to-culture protists: An effective approach to clarify biological interactions. *Environmental Microbiology* 2023; 1462-2920.16524.
21. Probert I, Siano R, Poirier C, Decelle J, Biard T, Tuji A, et al. *B randtodinium* gen. nov. and *B . nutricula* comb. Nov. (Dinophyceae), a dinoflagellate commonly found in symbiosis with polycystine radiolarians. *J Phycol* 2014; **50**: 388–399.
22. Yuasa T, Horiguchi T, Mayama S, Takahashi O. *Gymnoxanthella radiolariae* gen. et sp. nov. (Dinophyceae), a dinoflagellate symbiont from solitary polycystine radiolarians. *Journal of Phycology* 2016; **52**: 89–104.
23. Mitra A, Caron DA, Faure E, Flynn KJ, Leles SG, Hansen PJ, et al. The Mixoplankton Database (MDB): Diversity of photo-phago-trophic plankton in form, function, and distribution across the global ocean. *J Eukaryotic Microbiology* 2023; **70**: e12972.
24. Decelle J, Stryhanyuk H, Gallet B, Veronesi G, Schmidt M, Balzano S, et al. Algal Remodeling in a Ubiquitous Planktonic Photosymbiosis. *Current Biology* 2019; **29**: 968-978.e4.
25. Decelle J, Veronesi G, LeKieffre C, Gallet B, Chevalier F, Stryhanyuk H, et al. Subcellular architecture and metabolic connection in the planktonic photosymbiosis between Collodaria (radiolarians) and their microalgae. *Environmental Microbiology* 2021; **23**: 6569–6586.
26. Michaels AF. Acantharian abundance and symbiont productivity at the VERTEX seasonal station. *J Plankton Res* 1991; **13**: 399–418.
27. Michaels AF. Vertical distribution and abundance of Acantharia and their symbionts. *Marine Biology* 1988; **97**: 559–569.
28. Faure E, Not F, Benoiston A-S, Labadie K, Bittner L, Ayata S-D. Mixotrophic protists display contrasted biogeographies in the global ocean. *ISME J* 2019; **13**: 1072–1083.
29. Suzuki N, Aita Y. Radiolaria: achievements and unresolved issues: taxonomy and cytology. *Plankton and Benthos Research* 2011; **6**: 69–91.
30. Lipsman V, Shlakhter O, Rocha J, Segev E. Bacteria Contribute Exopolysaccharides to an Algal-Bacterial Joint Extracellular Matrix. *bioRxiv* 2023.
31. Brisbin MM, Mitarai S, Saito MA, Alexander H. Microbiomes of bloom-forming *Phaeocystis* algae are stable and consistently recruited, with both symbiotic and opportunistic modes. *The ISME Journal* 2022; **16**: 2255–2264.
32. Strelkov AA, Reshetnyak VV. A New Life Form in Radiolarians. *Zoological Journal* 1959; **38**.
33. Suzuki N, O'Dogherty L, Caulet JP, Dumitrica P. New integrated morpho- and molecular systematic classification of Cenozoic radiolarians (Class Polycystinea) – suprageneric taxonomy and logical nomenclatorial acts, in O'dogherty L. (ed.), Catalog of Cenozoic radiolarians. *Geodiversitas* 2021; **43**: 405–573.
34. Berney C, Fréderic M, Henry N, Enrique L, De Vargas C, Eubank consortium. EukBank 18S V4 dataset. 2023. Zenodo.

638 35. Schneider CA, Rasband WS, Eliceiri KW. NIH Image to ImageJ: 25 years of image analysis.
639 *Nat Methods* 2012; **9**: 671–675.
640 36. Abràmoff MD, Magalhães PJ, Sunanda JR. Image Processing with ImageJ. *Biophotonics*
641 *International* 2004; **11**: 36–42.
642 37. Llopis Monferrer N, Foulon V, Elies P. Enhanced scanning electron microscopy images using
643 muscovite mica, an example with Rhizaria. *Microscopy Res & Technique* 2022; **85**: 2748–
644 2751.
645 38. Schloss PD, Westcott SL, Ryabin T, Hall JR, Hartmann M, Hollister EB, et al. Introducing
646 mothur: Open-Source, Platform-Independent, Community-Supported Software for
647 Describing and Comparing Microbial Communities. *Appl Environ Microbiol* 2009; **75**:
648 7537–7541.
649 39. Guillou L, Bachar D, Audic S, Bass D, Berney C, Bittner L, et al. The Protist Ribosomal
650 Reference database (PR2): a catalog of unicellular eukaryote Small Sub-Unit rRNA
651 sequences with curated taxonomy. *Nucleic Acids Research* 2013; **41**: D597–D604.
652 40. Jamy M, Biwer C, Vaulot D, Obiol A, Jing H, Peura S, et al. Global patterns and rates of
653 habitat transitions across the eukaryotic tree of life. *Nat Ecol Evol* 2022; **6**: 1458–1470.
654 41. Rognes T, Flouri T, Nichols B, Quince C, Mahé F. VSEARCH: a versatile open source tool
655 for metagenomics. *PeerJ* 2016; **4**: e2584.
656 42. Sandin MM, Renaudie J, Suzuki N, Not F. Beyond the stars of the ocean: Diversity and
657 evolution of Radiolaria. *In prep* .
658 43. Katoh K, Standley DM. MAFFT Multiple Sequence Alignment Software Version 7:
659 Improvements in Performance and Usability. *Molecular Biology and Evolution* 2013; **30**:
660 772–780.
661 44. Larsson A. AliView: a fast and lightweight alignment viewer and editor for large datasets.
662 *Bioinformatics* 2014; **30**: 3276–3278.
663 45. Capella-Gutiérrez S, Silla-Martínez JM, Gabaldón T. trimAl: a tool for automated alignment
664 trimming in large-scale phylogenetic analyses. *Bioinformatics* 2009; **25**: 1972–1973.
665 46. Kozlov AM, Darriba D, Flouri T, Morel B, Stamatakis A. RAxML-NG: a fast, scalable and
666 user-friendly tool for maximum likelihood phylogenetic inference. *Bioinformatics* 2019; **35**:
667 4453–4455.
668 47. Minh BQ, Schmidt HA, Chernomor O, Schrempf D, Woodhams MD, Von Haeseler A, et al.
669 IQ-TREE 2: New Models and Efficient Methods for Phylogenetic Inference in the Genomic
670 Era. *Molecular Biology and Evolution* 2020; **37**: 1530–1534.
671 48. Ronquist F, Teslenko M, Van Der Mark P, Ayres DL, Darling A, Höhna S, et al. MrBayes
672 3.2: Efficient Bayesian Phylogenetic Inference and Model Choice Across a Large Model
673 Space. *Systematic Biology* 2012; **61**: 539–542.
674 49. Bouckaert R, Vaughan TG, Barido-Sottani J, Duchêne S, Fourment M, Gavryushkina A, et
675 al. BEAST 2.5: An advanced software platform for Bayesian evolutionary analysis. *PLoS*
676 *Comput Biol* 2019; **15**: e1006650.
677 50. Douglas J, Zhang R, Bouckaert R. Adaptive dating and fast proposals: Revisiting the
678 phylogenetic relaxed clock model. *PLoS Comput Biol* 2021; **17**: e1008322.
679 51. Gernhard T. The conditioned reconstructed process. *Journal of Theoretical Biology* 2008;
680 **253**: 769–778.
681 52. FitzJohn R G. Diversitree: comparative phylogenetic analyses of diversification in R.
682 *Methods in Ecology and Evolution* 2012; **3**: 1084–1092.

53. Tackmann J, Matias Rodrigues JF, von Mering C. Rapid Inference of Direct Interactions in Large-Scale Ecological Networks from Heterogeneous Microbial Sequencing Data. *Cell Syst* 2019; **25**: 286–296.
54. Sandin MM, Romac S, Not F. Intra-genomic RRNA gene variability of Nassellaria and Spumellaria (Rhizaria, Radiolaria) assessed by Sanger, MINION and Illumina sequencing. *Environmental Microbiology* 2022; **24**: 2979–2993.
55. Hagberg A, Swart P, Schult D. Exploring network structure, dynamics, and function using NetworkX. 2008. Gäel Varoquaux, Travis Vaught, and Jarrod Millman (Eds), Pasadena, CA, USA, pp 11–15.
56. Csárdi G, Nepusz T, Müller K, Horvát S, Traag, Zanini F, et al. igraph for R: R interface of the igraph library for graph theory and network analysis (v2.0.1). 2024.
57. Shannon P, Markiel A, Ozier O, Baliga NS, Wang JT, Ramage D, et al. Cytoscape: a software environment for integrated models of biomolecular interaction networks. *Genome Res* 2003; **13**: 2498–504.
58. Biard T, Bigeard E, Audic S, Poulain J, Gutierrez-Rodriguez A, Pesant S, et al. Biogeography and diversity of Collodaria (Radiolaria) in the global ocean. *ISME J* 2017; **11**: 1331–1344.
59. Larsson ME, Bramucci AR, Collins S, Hallegraeff G, Kahlke T, Raina J-B, et al. Mucospheres produced by a mixotrophic protist impact ocean carbon cycling. *Nat Commun* 2022; **13**: 1301.
60. Anderson OR, Swanberg NR, Bennett P. Assimilation of symbiont-derived photosynthates in some solitary and colonial radiolaria. *Mar Biol* 1983; **77**: 265–269.
61. Yuasa T, Takahashi O. Ultrastructural morphology of the reproductive swarmers of Sphaerozoum punctatum (Huxley) from the East China Sea. *European Journal of Protistology* 2014; **50**: 194–204.
62. Banaszak AT, Iglestas-Prieto R, Trench RK. *Scrippsiella vellelae* sp. nov. (Peridiniales) and *Gloeokinium viscum* sp. nov. (PHYTODINIALES), Dinoflagellate symbionts of two hydrozoans (Cnidaria) [1, 2]. *Journal of Phycology* 1993; **29**: 517–528.
63. Anderson OR, Swanberg NR, Bennett P. An estimate of predation rate and relative preference for algal versus crustacean prey by a spongiose skeletal radiolarian. *Mar Biol* 1984; **78**: 205–207.
64. Swanberg NR, Caron DA. Patterns of sarcodine feeding in epipelagic oceanic plankton. *J Plankton Res* 1991; **13**: 287–312.
65. Dennett MR. Video plankton recorder reveals high abundances of colonial Radiolaria in surface waters of the central North Pacific. *Journal of Plankton Research* 2002; **24**: 797–805.
66. Sandin MM, Romac S, Not F. Intra-genomic rDNA gene variability of Nassellaria and Spumellaria (Rhizaria, Radiolaria) assessed by Sanger, MinION and Illumina sequencing. *bioRxiv* 2021; **24**: 2979–2993.
67. Llopis Monferrer N, Biard T, Sandin MM, Lombard F, Picheral M, Elineau A, et al. Siliceous Rhizaria abundances and diversity in the Mediterranean Sea assessed by combined imaging and metabarcoding approaches. *Front Mar Sci* 2022; **9**: 895995.
68. Brisbin MM, Brunner OD, Grossmann MM, Mitarai S. Paired high-throughput, in-situ imaging and high-throughput sequencing illuminate acantharian abundance and vertical distribution. 2020. Microbiology.
69. Leonelli FE, Bellacicco M, Pitarch J, Organelli E, Buongiorno Nardelli B, De Toma V, et al. Ultra-Oligotrophic Waters Expansion in the North Atlantic Subtropical Gyre Revealed by 21 Years of Satellite Observations. *Geophysical Research Letters* 2022; **49**: e2021GL096965.

70. Albouy C, Delattre V, Donati G, Frölicher TL, Albouy-Boyer S, Leprieur F. Global vulnerability of marine mammals to global warming. *Scientific Reports* 2020.
71. Benedetti F, Vogt M, Hofmann Elizondo U, Righetti D, Zimmermann NE, Gruber N. Major restructuring of marine plankton assemblages under global warming. *Nature Communications* 2021.
72. Trubovitz S, Lazarus D, Renaudie J, Noble PJ. Marine plankton show threshold extinction response to Neogene climate change. *Nat Commun* 2020; **11**: 5069.

Figure headers

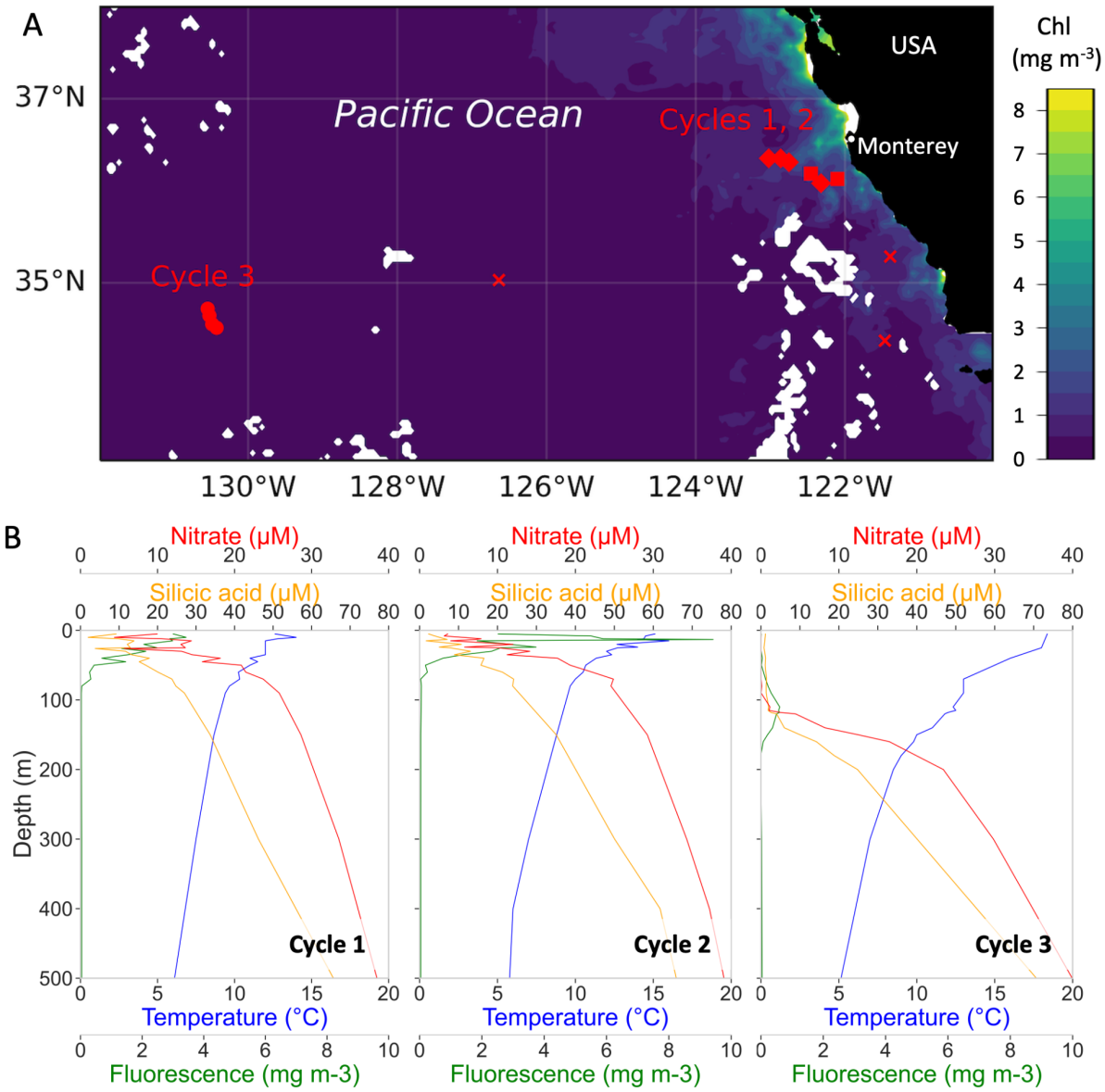

Fig. 1 (A) Map of the sampling locations of the P2107 cruise where net tows were carried out. Squares are used for Cycle 1, diamonds for Cycle 2, circles for Cycle 3 and crosses for sampling outside the cycles. Cycle 3 stations are where Nassellaria specimens used in this study were found. The color scale shows real time Aqua MODIS chlorophyll concentration (mg

m^{-3}), 4 km resolution for August 2021. **(B)** Fluorescence (mg m^{-3}) and temperature (°C) data from the CTD cast and nutrients concentration (silicic acid and nitrate, in µM) for each cycle.

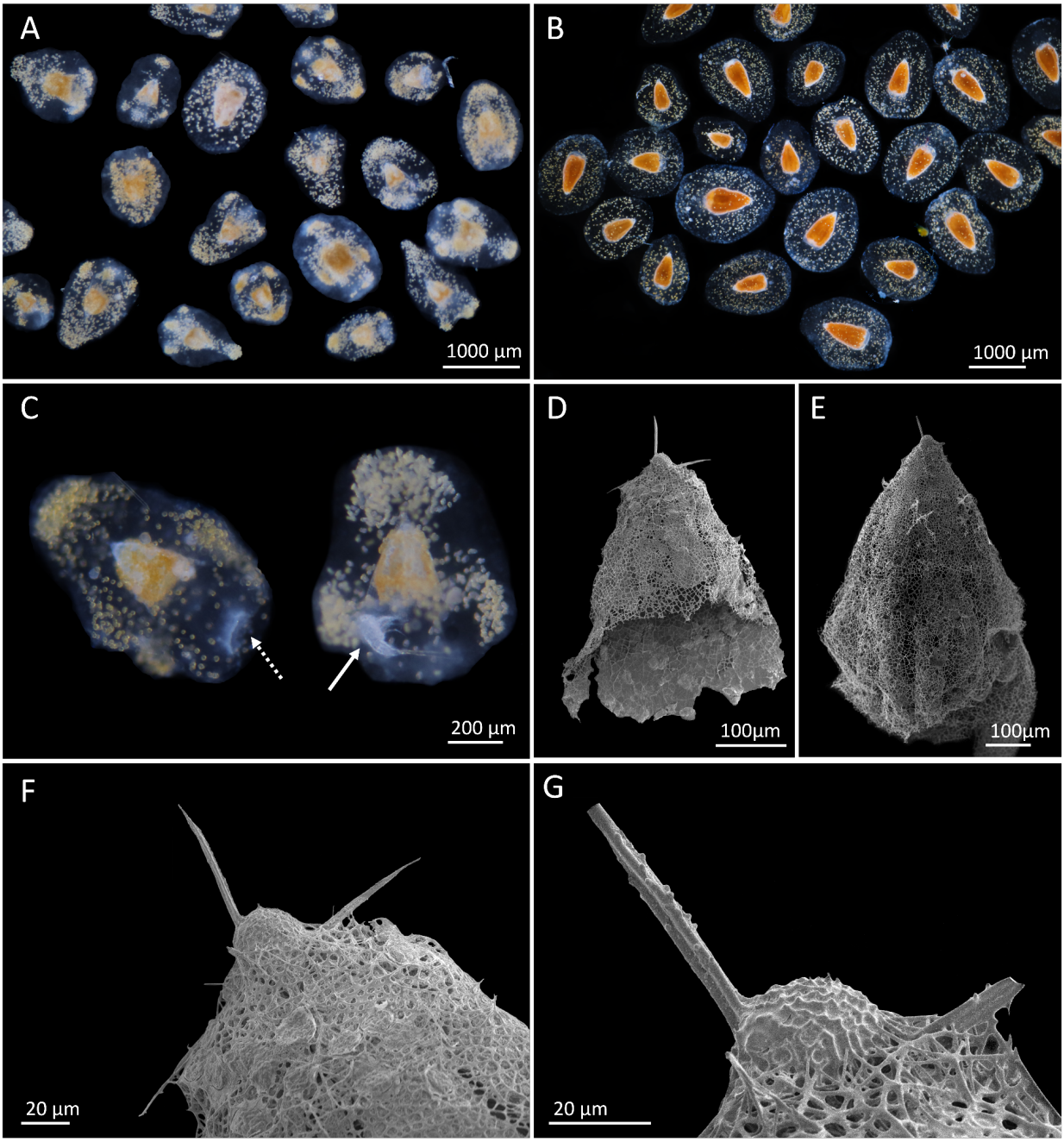

Fig. 2 (A-C) Light microscope images of living *Phlebarachnium* specimens; **C** is a composition of two separate images, with the dotted arrow indicating the aperture within the gelatinous matrix, and the solid arrow pointing to the prey embedded in the matrix, **(D-E)** scanning electron

749 micrograph of the skeleton of *Phlebarachnium* specimens, with a detailed focus of the cephalis
750 **(F-G)** used for traditional morphological classification. **A, C** and **E** are the "yellow" population of
751 *Phlebarachnium*. collected with the 0-50 m net tow; **B, C** and F are the "orange" population found
752 below 75 m.

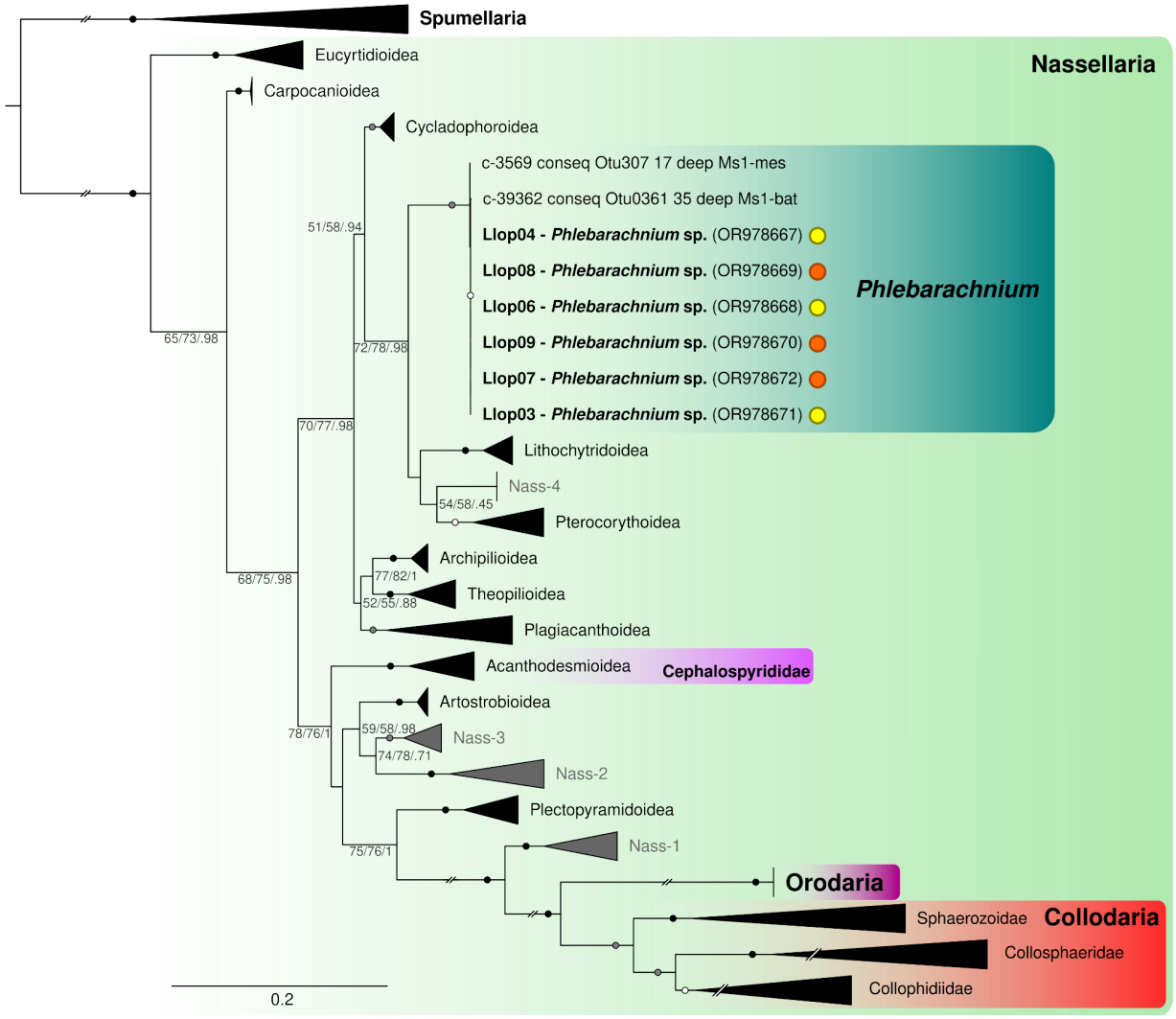

753

754 **Fig. 3.** Molecular phylogeny of Nassellaria inferred from the concatenated 18S and the partial
755 28S (D1+D2) rDNA (141 taxa and 2649 aligned positions), highlighting all described groups with
756 a gelatinous matrix. Note that within Acanthodesmioidea, only one family has been reported to be
757 surrounded by a gelatinous matrix (represented in our dataset by *Ceratospyris* and *Lophospyris).*
758 In total, 24 Spumellaria sequences were assembled as an outgroup. Values at nodes represent

759 RAxML-ng (GTR+Gamma; tree shown in figure), IQ-Tree (GTR+F+F4; 10 runs) bootstraps values
760 (BS; 1000 bootstrap each) and MrBayes (GTR+G) posterior probabilities (PP; computed after 10
761 million generations over 4 independent runs and 25% burnin). Only values above 50 BS and/or
762 0.5 PP are shown. Hollow circles at nodes indicate BS ≥ 80 and PP ≥ 0.8, filled grey circles BS ≥
763 90 and PP ≥ 0.9, and filled black circles BS ≥ 99 and PP ≥ 0.99. Branches and clades with a
764 double barred symbol have been 50% reduced for clarity. Orange and yellow circles after the
765 *Phlebarachnium* sequence names represent whether they belong to the so-called "orange" or
766 "yellow" populations.

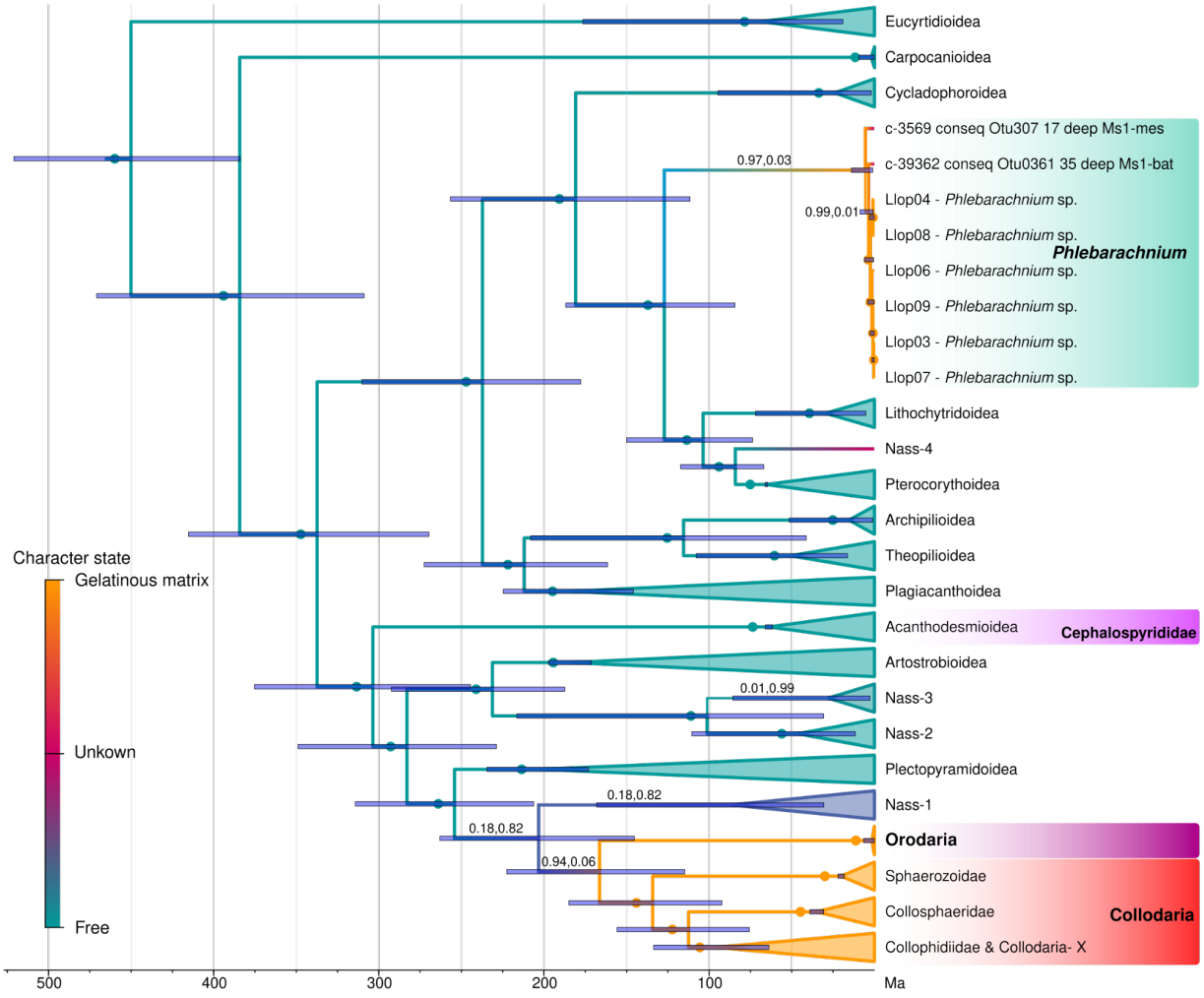

767

768 **Figure 4**. Time-calibrated tree (Molecular clock) of Nassellaria highlighting in the branch color the
769 ancestral state reconstruction probabilities between a state with presence of a gelatinous matrix

or absence (free). Divergence times were inferred under an optimized relaxed clock model and GTR+G for 3 independent chains of 100M cycles sampled every 1000 steps and a 25% burnin, implemented in the software package BEAST2, on the alignment matrix used for phylogenetic analyses (Fig. 3). Twelve different nodes were selected for the calibration, based on [40] with the exception of the root in which a uniform distribution (with minimum of 500 and maximum of 1200 Mya) was used. Ancestral state reconstruction was performed under a binary state speciation and extinction model (BiSSE) implemented in the R package *diversitree*. Values above branches represent the probability of a gelatinous ancestral state and of the absence of a gelatinous matrix respectively. When full support for either state, probabilities are represented by a dot. Blue bars indicate the 95% highest posterior density (HPD) intervals of the posterior probability distribution of node ages.

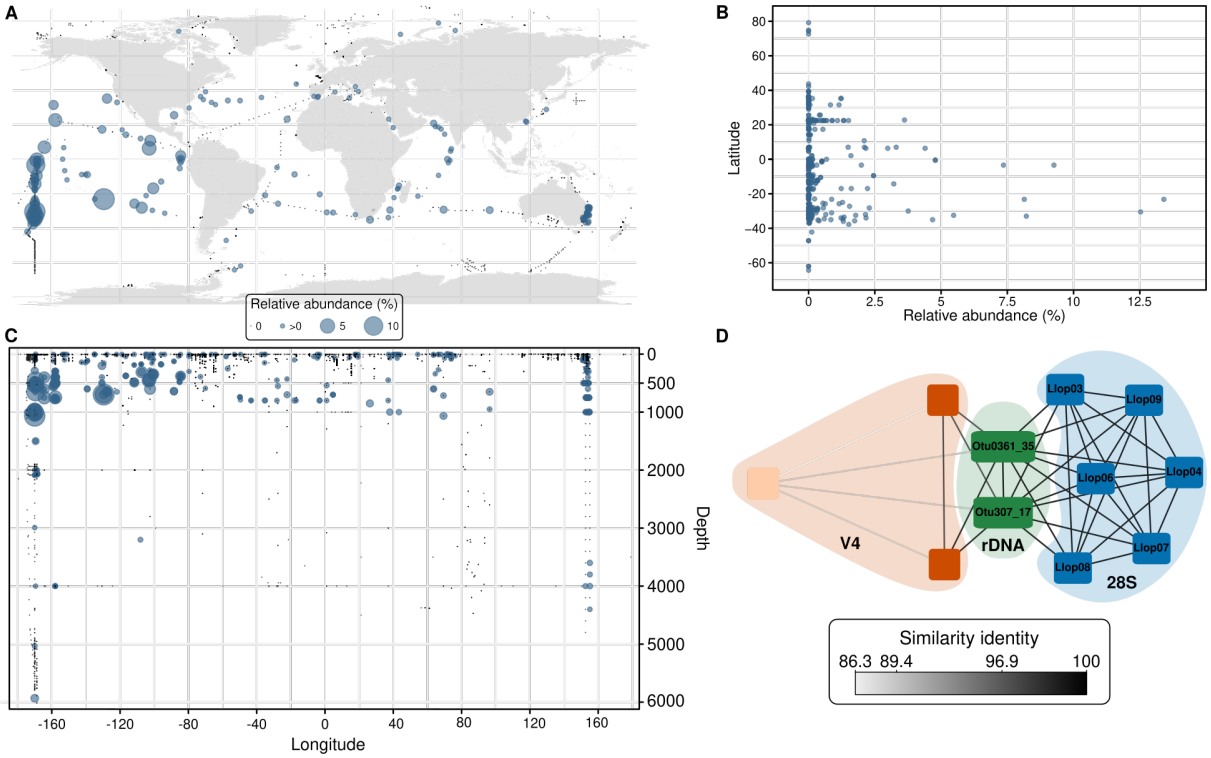

Fig. 5 Global biogeography of *Phlebarachnium*. inferred from the EukBank dataset (Berney et al. 2023) on samples with a marine identifier. **(A)** World map showing the different sampling stations

784 (black dots) and maximum contribution of *Phlebarachnium*. to the total eukaryotic community
785 (blue dots) per locality. **(B)** Relative abundance of *Phlebarachnium*. across the latitudinal gradient.
786 **(C)** Depth profile of *Phlebarachnium*. across the longitudinal gradient. Note panels A, B and C are
787 aligned so that latitude and longitude can be cross-linked (a very dimmed grid can be seen in
788 panel A for the main parallels and meridians extended from panels B and C respectively). **(D)**
789 Graphical representation of the similarity identity (computed with vsearch: 'allpairs_global'; and
790 represented by the grey gradient lines, or edges) between all *Phlebarachnium* sequences
791 (coloured squares, or nodes) used in this study. Blue nodes represent the D1+D2 regions of the
792 28S rDNA sequenced in this study, green nodes represent the near full-length rDNA, and orange
793 represent the V4 hypervariable region of the 18S rDNA from eukBank [34]. Note the light orange
794 node representing the third closest hit to our reference sequences, and confidentially showing the
795 taxonomic assignment of *Phlebarachnium* used in this study. Node codes refer to the sequence
796 identifier for referencing across figures (e.g. Fig. 3)).

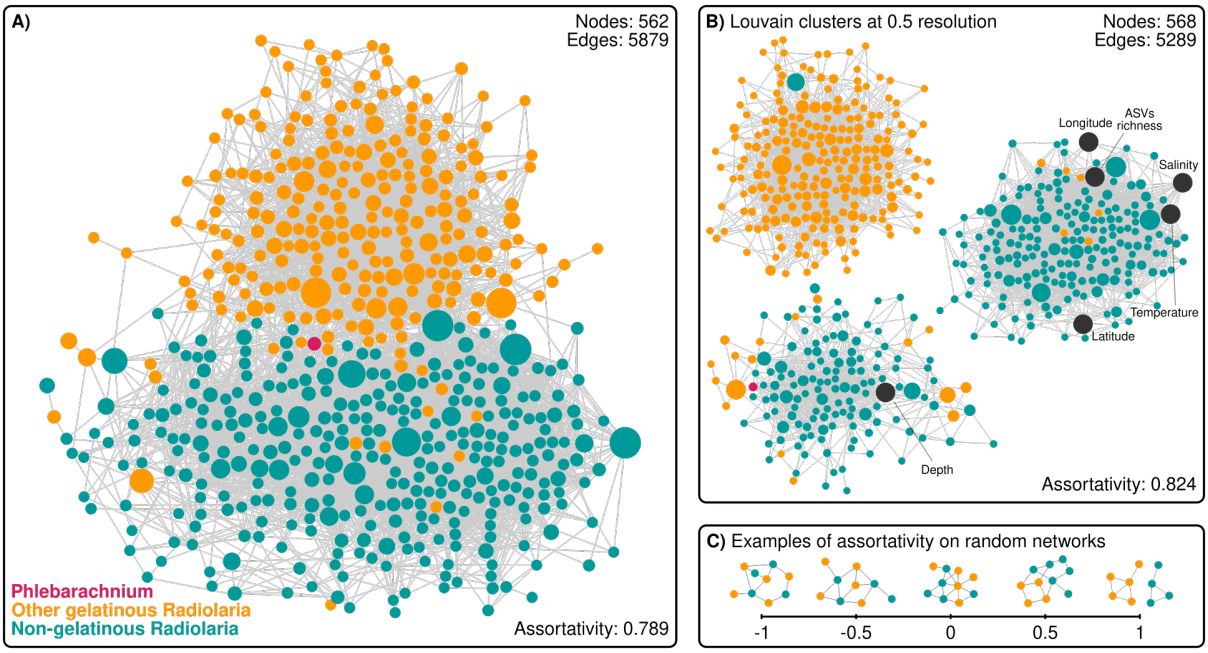

797

798 **Figure 6**. **A)** Co-occurrence network of Radiolaria across the global oceans highlighting
799 gelatinous and non-gelatinous amplicons (nodes) extracted from the EukBank dataset. Co-
800 occurrence was estimated in FlashWeave, including only amplicons with a maximum relative
801 abundance (to any given sample) of at least 1%, in order to remove co-occurrence of sequencing
802 errors and other artifacts, and amplicons whose gelatinous attribute is known (please see **SupMat**
803 **Fig. S3**, for a detailed co-occurrence of different size fractions and **SupMat fig S4** for co-
804 occurrence analysis of amplicons with both known and unknown attributes). For clarity, negative
805 connections and environmental variables were removed from the graph. **B)** Louvain clusters of
806 the original network shown in A) (including negative connections and environmental variables)
807 explaining community structure and co-occurrence. Environmental variables are shown in dark
808 gray circles. Size of the nodes represent the maximum relative abundance for visual guidance.
809 **C)** Random networks with given attributes to exemplify different levels of assortativity.

810 Supplementary Material table headers

811 **Table S1**. Morphological measurements, major and minor axes of individual cells, and their
812 skeleton and gelatinous matrix areas.
813 **Table S2**. List of specimens used for phylogenetic analysis.

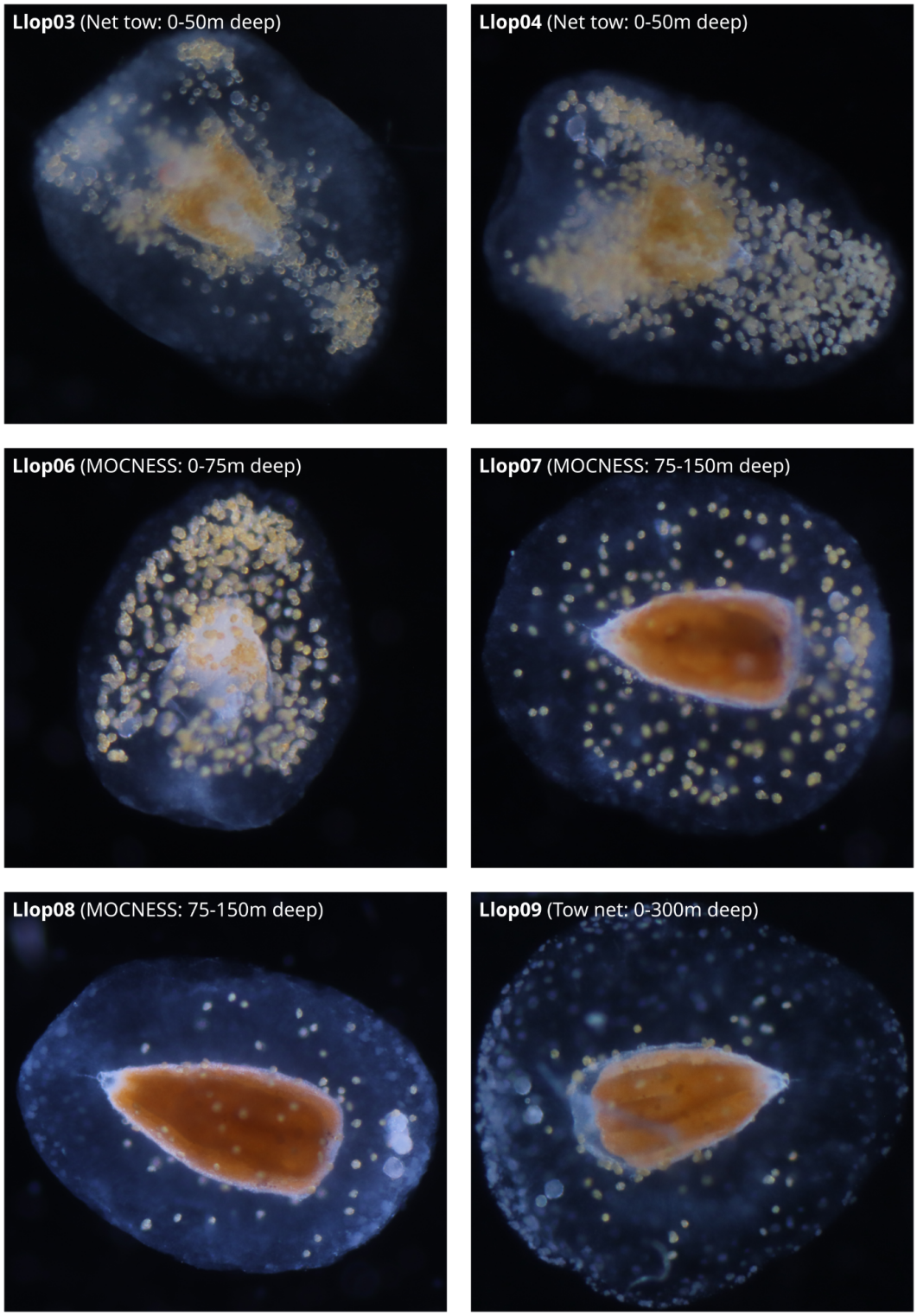

Figure S1. Light microscope images of live *Phlebarachnium* specimens used in this study for phylogenetic analysis in Fig. 3. Scale bar represents 500 μm.

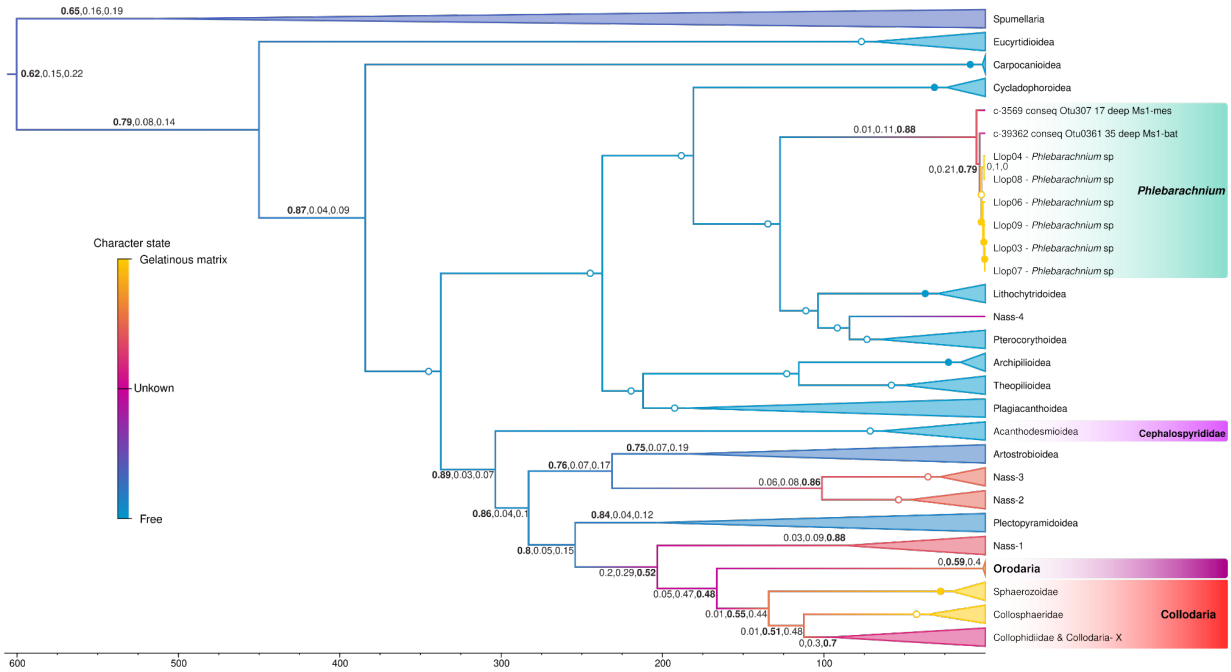

Figure S2. Bayesian ancestral state reconstruction performed under a birth death model implemented in BEAST2 with 10 million generations sampled every 1000 steps and a 25% burnin. Values above branches represent the probability of the absence of a gelatinous matrix ancestral state, of a gelatinous matrix ancestral state and of an unknown state (considered as a third state methodologically) respectively. When full support for either state, probabilities are represented by a full circle. Hollow circles represent posterior probabilities equal or bigger than 0.90 for the given state and smaller than 0.05 for the two other states.

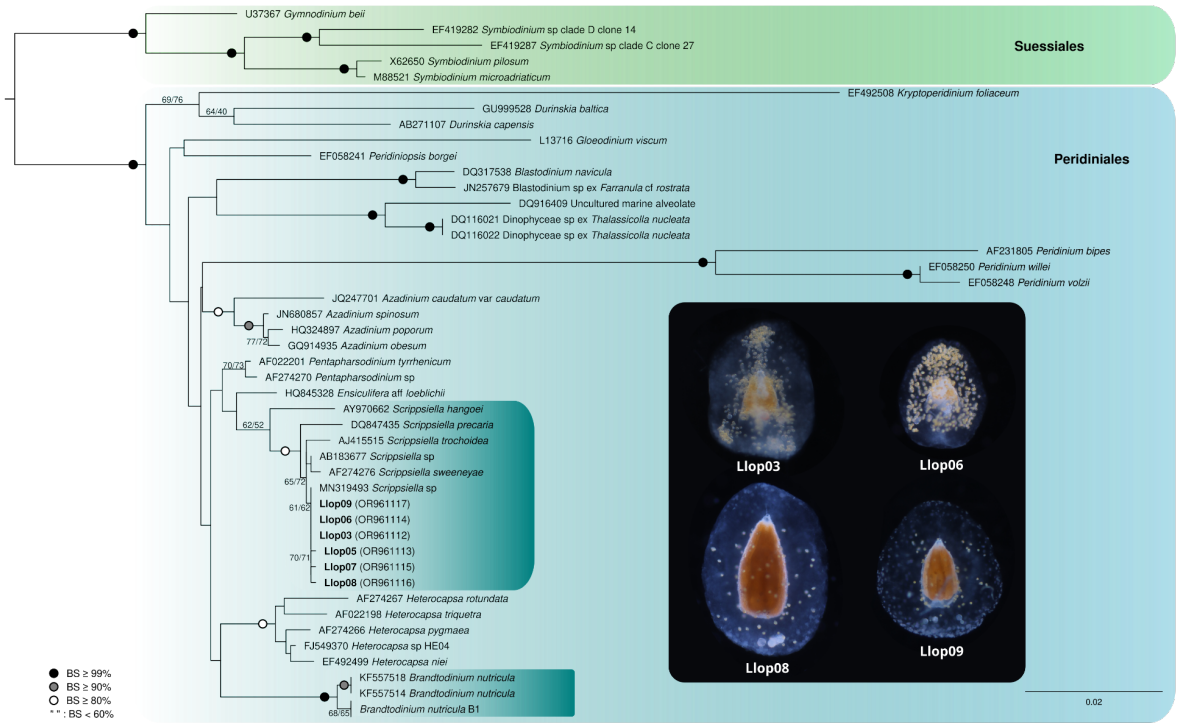

Figure S3. Molecular phylogeny of Perinidiales, with special focus on symbiotic dinoflagellates inferred from the 18S rDNA (71 taxa and 1803 aligned positions) using the sequences published in [21] as reference. Values at nodes represent RAxML-ng (GTR+Gamma; tree shown in figure), IQ-Tree (GTR+F+F4; 10 runs) bootstraps values (BS; 1000 bootstrap each). Only values aboce 60 BS are shown. Hollow circles at nodes indicate BS ≥ 80, filled grey circles BS ≥ 90 and filled black circles BS ≥ 90 and filled black circles BS ≥ 99.

A) Small size fractions (0.22 - 20 µm)
Nodes: 547
Edges: 1950
Assortativity: 0.749
B) Louvain clusters at 0.5 resolution
Nodes: 547
Edges: 1651
ASVs richness
Temperature
Latitude
Salinity
Longitude
Depth
Assortativity: 0.869
C) Medium size fractions (3 - 200 µm)
Nodes: 489
Edges: 925
Assortativity: 0.646
D) Louvain clusters at 0.5 resolution
Nodes: 480
Edges: 727
Salinity
Longitude
Latitude
Temperature
ASVs richness
Depth
Assortativity: 0.684
E) Big size fractions (80 - >2000 µm)
Nodes: 454
Edges: 844
Assortativity: 0.734
F) Louvain clusters at 0.5 resolution
Nodes: 438
Edges: 714
Salinity
Temperature
Longitude
Latitude
ASVs richness
Assortativity: 0.775

832

833 **Figure S4**. Detailed size-fraction co-occurrence networks of Radiolaria across the global
834 oceans highlighting gelatinous and non-gelatinous amplicons (nodes) extracted from the
835 EukBank dataset shown in **Fig. 6**. Left panel (A, C, D) shows the different arbitrary size-
836 fractions and corresponding louvain clusters on the right panel (B, D, E, respectively). For
837 further details, see **Fig. 6** legend.

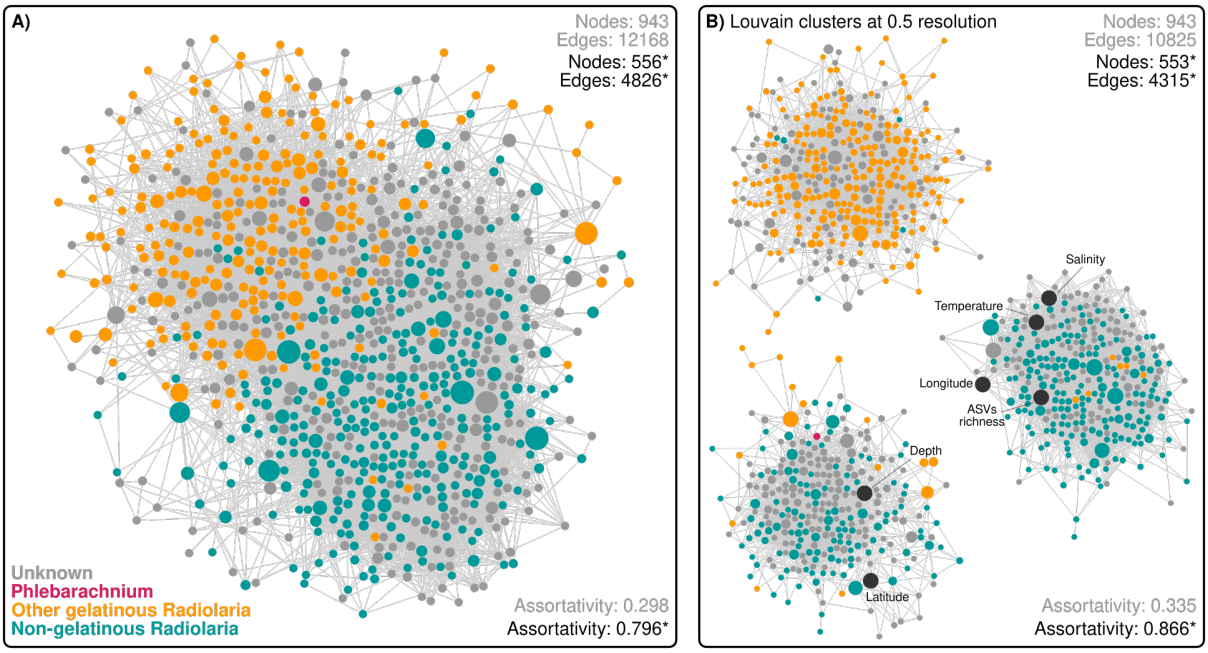

838

839 **Figure S5**. **A**) Co-occurrence network of Radiolaria across the global oceans highlighting
840 gelatinous and non-gelatinous amplicons (nodes) extracted from the EukBank dataset and
841 including amplicons whose morphology remains unknown. **B**) Louvain clusters of the original
842 network shown in A) explaining community structure and co-occurrence. Given that assortativity
843 is property of nodes with given attributes, the absence of attribute is interpreted as a third
844 attribute, and thus assortativities are given for the shown graph (in gray) and for the same graph
845 after removing nodes with unknown attributes (in black, with an asterisk).

846